Programmable mechanical metamaterials

Florijn, H.C.B.

CHAPTER 5

BARCODE METAMATERIAL

In the previous chapters we have studied the mechanical response of a laterally confined 5×5 biholar sample under uniaxial loading. Sofar, the clamps that laterally confine the samples were placed on all rows that terminate in small holes, and the confinement was thought of as a homogeneous field characterized by a single parameter. It is thus natural to ask what happens when either rows that terminate in large holes are clamped, or when the clamping becomes strongly inhomogeneous. In this chapter we present a systematic study of the effect of clamping details on the mechanical response and programmability of biholar metamaterials. We find that clamping leads to inhomogeneities in the materials polarization, which can cause sharp domain walls to form between x- and y-polarized patches. These domain walls can either propagate through the bulk or get trapped near the boundary, and this behavior can be controlled by the precise clamping conditions. This leads to a complete new "barcode" programmability of our biholar metamaterials, where the location or absence of clamps at certain locations can be used to strongly influence the mechanical response of our materials to uniaxial compression.

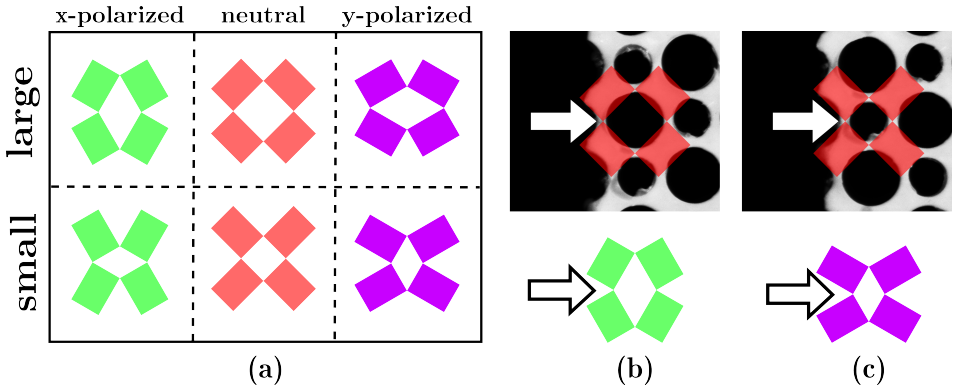

FIGURE 5.1: (a) Orientation of the mechanism around a small hole or a large hole when polarized in the x- or y-direction. (b) Mechanism drawn on top of a large boundary hole. When confined, the large boundary hole will become x-polarized. (c) Mechanism drawn on top of a small boundary hole. The small hole will become y-polarized.

5.1 Motivation

The crucial physics underlying the programmability of biholar metamaterials is the broken rotational symmetry which sets up a competition between x and y polarized patterns, driven by the lateral confinement and uniaxial compression. So far, we have considered small samples, whose behavior can be captured by a single polarization quantity, despite their obvious spatial inhomogeneities. However, even for these small samples, a careful inspection of the spatial structure of their deformation and polarization suggests that gradients must play a role. Moreover, the precise details of the clamping conditions, and in particular the question whether a clamped row of holes terminates in a large or a small hole is important. In Fig. 5.1 we illustrate the effect of homogeneous and inhomogeneous confinement on mechanisms describing the terminating small (large) hole along the left edge of a biholar sample. In panel (a) we recall the local configuration of the biholar mechanism around a small and a large hole, both for a x- and y-polarized state. The crucial observation regarding the edge holes is that the local force exerted on the corresponding mechanisms is localized near the left hinge of the mechanism — very different from the forcing along the springs as shown in Fig. 3.2.

In Fig. 5.1(b) we consider what happens when a small hole is laterally confined, and in Fig. 5.1(c) we show the same consideration for a large hole. Despite the fact that in both cases the clamping pushes 'inward' along the x direction, we find that the small hole actually gets y-polarized, whereas the large hole gets x polarized. However, far away from the boundary, in both cases the pattern will be x-polarized. This suggest that there is a difference between s-clamping (clamping a small hole) and l-clamping (clamping a large hole): for s-clamping, the x-polarization will be strongest in the bulk, with a boundary zone which tends to be y-polarized, whereas for l-clamping, the x-polarization will be more homogeneous (although often stronger at the boundary). Below we will show in detail that this picture, despite its simplicity, captures the more complex deformations in realistic soft samples.
The mechanical response under uniaxial y compression depends now on how the differently polarized regions of the sample respond, and in particular, how the bulk and boundary region are different. As we will show below, this leads to a very rich spatial dynamics of differently polarized patches in our samples, with often sharp domain walls which can move through the sample in response to a change in compression, thus resulting in highly complex mechanical behavior.

5.2 Programmable mechanics by position of the clamps

In this section we will study the effect of the position of a single confining clamp on the mechanical response of 5×5 biholar sample with $D_1 = 10$ mm, $D_2 = 7$ mm, pitch $p = 10$ mm ($\chi = 0.3$ and $t = 0.15$) and depth $d = 35$ mm to avoid out of plane buckling. As in section 4.2 the compressive vertical strain is defined as

$$\varepsilon_y = \frac{2u_y}{L_{y1} + L_{y2} + 2t'} \tag{5.1}$$

As before, we impose lateral confinement by fixing the distance between copper rods, glued to the lateral sides of the sample, with laser cut transparent (PMMA) clamps. The global confining strain is defined as $\varepsilon_x = 1 - L_c/L_{c0}$, with L_{c0}, the distance between the metal rods in the unconfined state being different for odd and even rows. For odd rows, which terminate with large holes, from now called ll-rows: $L_{c0} = 6p - D_2 = 53$

mm, while for even rows, which terminate small holes (*ss*-rows): $L_{c0} = 6p - D_1 = 50$ mm.
In our experiments we measure the force F, which is expressed as the dimensionless stress S (see Eq.(4.2)), as a function of compressive strain ε_y. Shown in Fig. 5.2 are the $S(\varepsilon_y)$-curves for 11 different values of ε_x, ranging from $\varepsilon_x = 0.14$ to $\varepsilon_x = 0.34$, for (a) a single clamp placed on a *ss*-row ($row = 4$) and (b) a single clamp placed a *ll*-row ($row = 3$) (see inset).
In Fig. 5.2(a) we recognize the different mechanical regimes encountered before; the monotonic regime (*i*) for $\varepsilon_x \leq 0.16$, the non-monotonic regime (*ii*) for $0.18 \leq \varepsilon_x \leq 0.20$, and the hysteretic regime (*iii*) for $\varepsilon_x > 0.20$. Note that more horizontal strain is needed to reach the (*i*)-(*ii*)-transition and the (*ii*)-(*iii*)-transition when using a single clamp than when both *ss*-rows are confined, see Fig. 2.17.
In Fig. 5.2(b) the trends in $S(\varepsilon_y)$ with increasing ε_x are less pronounced. For $\varepsilon_x = 0.14$ $S(\varepsilon_y)$ is monotonic. Then increasing ε_x, $S(\varepsilon_y)$ becomes non-monotonic with a large range of negative incremental stiffness for $\varepsilon_x = 0.24$. Curves with $\varepsilon_x > 0.24$ show hysteric behavior which is less pronounced than observed for samples confined at the *ss*-rows. There is a clear difference in phenomenology of the mechanical response between the samples confined at the *ss*- or *ll*-rows.

To better understand the role of the boundary holes, in Fig. 5.3 we show the $S(\varepsilon_y)$-curves for $\varepsilon_x = 0.26$ where in (a) the clamp is located at a *ss*-row and in (b) the clamp is located at a *ll*-row. Indicated in the figures are six points, marked by the numbers (1)-(6) corresponding to the two times six images below.
As we will show now, there are significant differences between the sequence of patterns for *ss*-clamps (Fig. 5.3(a)) and *ll*-clamps (Fig. 5.3(b)). Recall, we call a pattern x-polarized when the major axis of the large holes are orientated vertically and the major axis of the small holes are orientated horizontally and y-in the opposite case (see Fig. 5.1). Even though the patterns are highly complicated and heterogeneous for large confinements, the orientation of individual holes is sufficient to determine whether a patterns is locally x- or y-polarized.
At (1), $\varepsilon_y = 0$, the pattern in the bulk is x-polarized, with significant distortion near the confined boundaries where the pattern is locally close to the y-polarized state, consistent to what was suggested in section 5.1. At

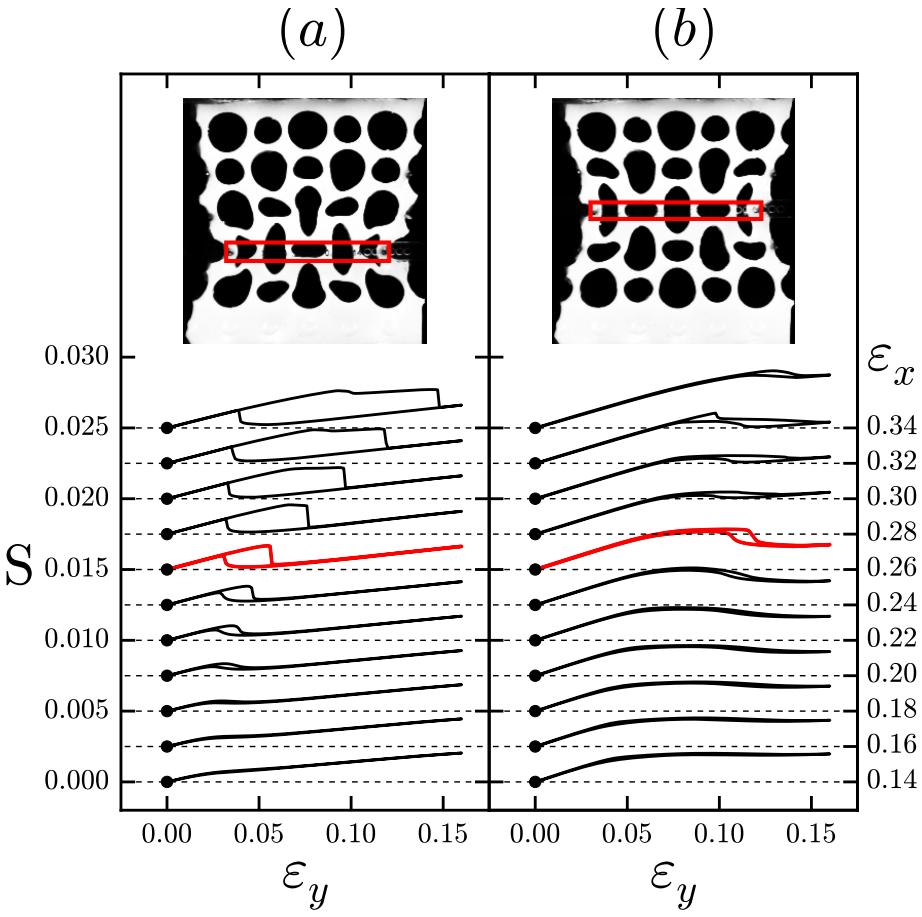

FIGURE 5.2: $S(\varepsilon_y)$-curves for a biholar sample with $\chi = 0.3$, $t = 0.15$ for a range of lateral confining strains ε_x (indicated right) where a single clamp is placed on (a) a even *ss*-row ($row = 4$) and (b) an odd *ll*-row ($row = 3$). Curves offset for clarity.

(2), $\varepsilon_y = 0.056$ at the top of the peak of the hysteretic curve, the top part of the sample is essentially neutral (due to the stiff top boundary), while the bottom three rows are strongly x-polarized, except for the two small boundary holes, which are strongly y-polarized. At (3), $\varepsilon_y = 0.057$, after the stress jump, the pattern has switched to a fairly homogenous y-polarized state. When ε_y is increased further (4), it becomes even more y-polarized. Decompressing the system, (5), $\varepsilon_y = 0.038$, the y-polarization

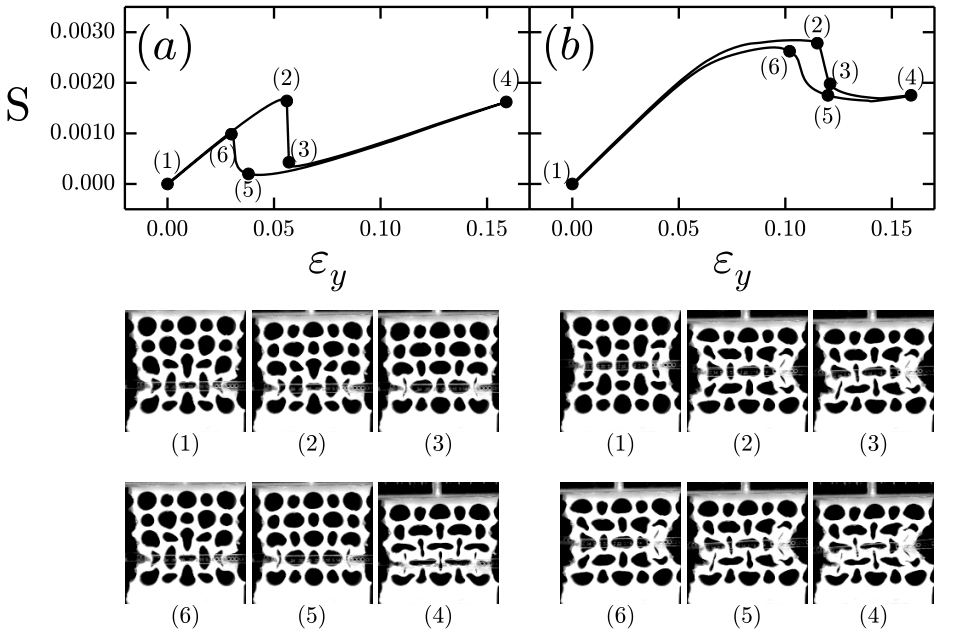

FIGURE 5.3: $S(\varepsilon_y)$-curves for a biholar sample with $\chi = 0.3$, $t = 0.15$ for $\varepsilon_x = 0.26$ where a single clamp is placed on (a) a *ss*-row ($row = 4$) and (b) a *ll*-row ($row = 3$). Indicated in each figure are six points corresponding to the six images below.

becomes less strong and the system jumps back to being x-polarized at (6), except for the two small boundary holes. Hence in this case, despite vertical gradients and distortions near the clamps, the overall state of the system can be captured by its overall polarization, which distinguishes the upper and lower branch of the hysteretic cycle.

Confining a *ll*-row as in Fig. 5.3(b) results in a significantly different mechanical response, Fig. 5.3(b). The $S(\varepsilon_y)$-curve displays hysteresis but is less pronounced than for a *ss*-row confinement. Moreover,the maximal compressive stresses are larger then for *ss*-row confinements: in Fig. 5.3(a) the maximum value of the peak is $S = 0.0018$, while in Fig. 5.3(b) the maximum of S is $S = 0.0030$ for $\varepsilon_x = 0.26$.

At (1), the *entire* pattern is x-polarized. Note that the x-polarization is strongest near the confined large boundary holes, again consistent with the scenario sketched in section 5.1. At (2), most of the pattern has become y-polarized, with the exception of the area near the clamps (in par-

ticular the right clamp, which is strongly x-polarized) where the strain has strongly localized and the system is highly deformed. Between (1) and (2) the pattern in the bulk has smoothly changed from overall x-polarized to overall y-polarized, without notable events in the S-curve.
At (3), after the stress jump, no significant changes in the pattern are observed, with the exception of the left terminating beam on row 4. Notice that the clamp is slightly tilted as the left big boundary hole at the confined row is pushing outward forcing the clamp on this side of the sample to move downward. This symmetry breaking is better visible at (4), where the pattern is even more compressed and the shape of the left big boundary hole in the confined row is close to a y-polarized ellipse, as opposed to the case of small ε_y. The large confined boundary hole to the right remains strongly x-polarized. The stress jump between (2) and (3) is related to the rapid change of sign (snapping) of the curvature of the beam adjacent to the left terminating hole.
From (4)-(6), decompressing the system, the pattern smoothly becomes less compressed. Although the stress increases between (5)-(6), changes in the pattern are minor, and concentrated near the left terminating beam on row 4.
We conclude that placing the clamp on a row starting and ending with a large hole (ll-rows) in a 5×5 biholar sample results in additional frustration, particularly near the boundaries. The overall pattern smoothly changes its polarization, except for the region near the left confined large hole. The region near the right confined large hole remains x-polarized for the full compression-decompression sweep. Notable events in the $S(\varepsilon_y)$-curves are due to events occurring at the (left) boundary of the system. This is in contrast to a 5×5 biholar sample that is confined at ss-rows, where the pattern rapidly changes from a fairly homogenous x-polarized to a y-polarized state, and the corresponding jump in stress can be directly related to this pattern change in the bulk of the sample.
Let us now discuss our findings in the light of the framework outlined in Fig. 5.1. A first prediction is that, for $\varepsilon_y = 0$, there should be a significant difference in the polarization of the boundary region near the clamps between ss-clamps and ll-clamps. Indeed, we observe in Fig. 5.3 that for ss-clamps, the near-boundary region is somewhat ambiguous, whereas for ll-clamps, the whole sample is clearly x-polarized. Second, we predicted that the x polarization of the clamped row would be function of x, with the

maximum x-polarization in the bulk for ss-clamping, and the maximum x-polarization near the edges for ll-clamping: while the former is hard to detect in these small samples, the latter appears to be correct. Third, the gradient in polarization for $\varepsilon_y = 0$ may persist for larger vertical compressions — here our small samples are too small to see convincing differences between ss- and ll-clamping. To probe in more detail the differences between ss- and ll-clamping, in the following we will turn our attention to larger systems, in which all predicted trends will be clearly present.

Large System heterogeneous clamping

To clearly distinguish events occurring at the boundary of the system and in the bulk, we increase the system size. Again we use a biholar sample with $\chi = 0.3$ and $t = 0.15$ ($D_1 = 10$ mm, $D_2 = 7$ mm, $p = 10$ mm, d = 35 mm) but now with 9 holes in the horizontal direction and 10 holes in the vertical direction. With 10 holes in the vertical direction the compressive vertical strain definition (Eq. 5.1), uses $L_{y1} = 9p + D_1$ and $L_{y2} = 9p + D_2$. With 9 holes in the horizontal direction, the dimensionless stress S is now defined as:

$$S := \frac{\sigma_y}{E}\frac{A_{\text{eff}}}{A} = \frac{10t'F}{dE(L_x + 2t')^2}\,, \tag{5.2}$$

where the width of the top row is given by $L_x = 9p + D_1$. Moreover, the distance between the metal rods without clamps L_{c0} is $L_{c0} = 10p - D_2 = 93$ for ll-rows, or $L_{c0} = 10p - D_1 = 90$ mm for ss-rows.

Shown in Fig. 5.4 are the S-curves of a uniaxially compressed biholar sample with lateral confinement $\varepsilon_x = 0.20$. Indicated in each graph are six points: (1) the start of the experiment at $S(\varepsilon_y = 0) = 0$; (2)-(3) the location of the jump during compression of the sample; (4) the maximum applied strain and, (5)-(6), the location of the jump while decompressing the sample. Below each graph are six images corresponding to the six points indicated in the figure. The colors of the fields drawn, by hand, on top of each image indicate the polarization of the domains; green for x-polarized domains, purple for y-polarized domain. The white arrows indicate the location of the (transparant) clamps.

In Fig. 5.4(a) the clamp is placed on row 6 (ss-row) while in Fig. 5.4(b) the clamp is placed on row 5 (ll-row). Both S-curves exhibit hysteresis, however the locations of the stress jumps differ. In Fig. 5.4(a) the jump to a lower branch, indicated by (2) and (3), is at $\varepsilon_y = 0.06$, while in Fig. 5.4(b)

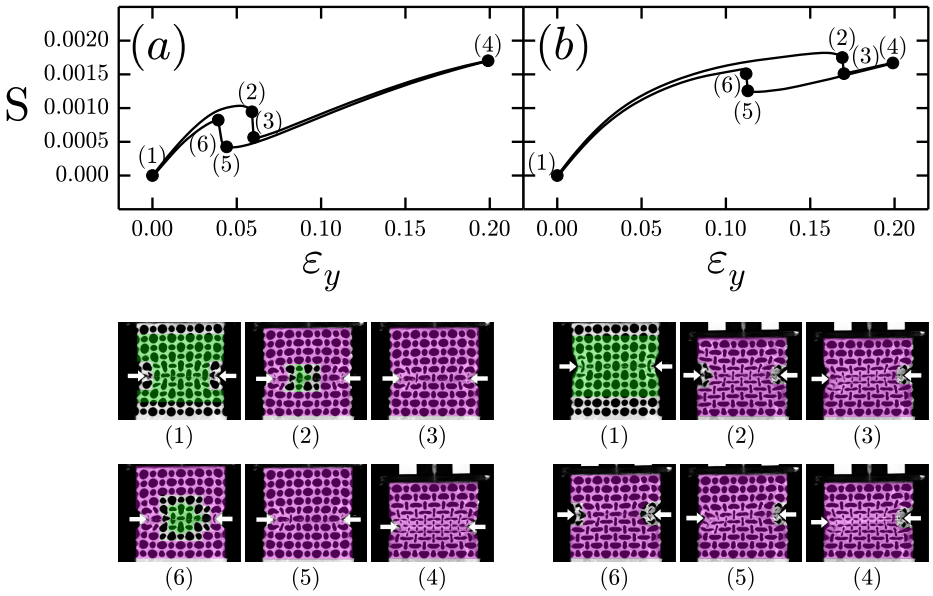

FIGURE 5.4: A 9×10 biholar sample with $\chi = 0.3$ and $t = 0.15$ confined with a single clamp. (a) Confining ($\varepsilon_x = 0.20$) *ss*-row 6, a row terminating in small holes ($D_2 = 7$ mm). (b) Confining *ll*-row 5, a row terminating large holes ($D_1 = 10$ mm) with $\varepsilon_x = 0.20$. Indicated in each top panel are six points corresponding to the six images in the lower panels. The color denotes the polarization of the pattern, green for *x*-polarized, purple for *y*-polarized. The location of the (transparent) clamp is indicated by the white arrows.

this occurs at $\varepsilon_y = 0.17$. Decompressing the sample, the jump in stress, indicated by (5) and (6), takes place at $\varepsilon_y = 0.04$ in Fig. 5.4(a) and at $\varepsilon_y = 0.11$ in Fig. 5.4(b).

The nature of the pattern change, as observed from the colored images, depends on which type of row is confined (*ss*-row or *ll*-row). Shown in Fig. 5.4(a), initially (1) the pattern is fully *x*-polarized (purple), except for the small boundary holes adjacent to the confining clamp, which are not colored since their polarization is ambiguous. Note that the polarization is strongest in the center of the confined row, consistent with the scenario sketched in section 5.1. Arriving at the jump (2), almost the entire pattern has smoothly (no visible stress jumps in the *S*-curve and no sudden pat-

tern changes) changed polarization, except for a small region in the middle of the sample, centered around row 6. Around this small y-polarized region there is a domain wall, with a width not larger than a single hole, consisting of highly frustrated holes, where the pattern is neither x- nor y-polarized and the holes have shapes best described as triangles. Note that the regions near the confined boundary holes are no colored purple as these parts are now clearly y-polarized. As shown in image (3), for larger compression, the entire pattern is now y-polarized. Hence, the jump in stress between (2) and (3) coincides with the disappearance of a x-polarized domain in the *bulk* of the sample. At image (4) the sample is fully compressed to $\varepsilon_y = 0.20$ and the pattern is strongly y-polarized. Note that the polarization of the holes nearest to the confining clamp is the strongest. Decompressing the sample, arriving at (5), the pattern is fully y-polarized. Between (5) and (6), a large region in the middle of the sample, centered around row (6), changes polarization. A domain wall of highly frustrated holes is surrounding this x-polarized purple region. Hence, the sudden increase of stress between (5) and (6) in the S-curve coincides with the appearance of a x-polarized domain in the bulk of the sample.

The scenario shown in Fig. 5.4(b) is qualitatively different. Initially at (1), the *entire* pattern is x-polarized, including the boundary region near the confined boundaries. Note that the polarization is strongest at these boundary holes and decreases towards the center of the sample, consistent with the scenario sketched in section 5.1. Then, arriving at (2), the entire sample has smoothly changed polarization, except a small region at the left boundary of the sample, near the clamp. In this region the holes are neither x- nor y-polarized, with shapes hard to characterize. Note that the holes at the right boundary near the clamps are fully closed. Upon further compression, there is a small stress jump, and as shown in image (3), the pattern is now fully y-polarized, including the left confined boundary hole. Moreover, the arrows in image (3), indicating the location of the clamp confining the sample, are not aligned anymore, i.e. the clamp is skewed. The jump in stress in the S-curve thus coincides with the disappearance of the highly frustrated region near the clamp contact.

At image (4), the pattern is fully compressed and strongly y-polarized. Decompressing the sample, and arriving at the jump located between (5)-(6), we see that a small highly frustrate region at the left region of the sample

near the clamp emerges. Hence, the sudden increase of stress between (5) and (6) in the S-curve coincides with the appearance of a highly frustrated region at the boundary of the sample.
To summarize, Fig. 5.4 shows a clear distinction between confining ss-rows or ll-rows. For ss-row confinement, initially the sample is x-polarized, except for the regions near the confining clamp. The initial polarization is strongest in the center of the sample, the region that, for increasing uniaxial compression, eventually will discontinuously change polarization to y, in agreement with the framework presented earlier. In a 9×10 sample this clamping configuration will result, for large enough confinements, in stress jumps in the S-curve at low vertical strains coinciding with changes of polarization of domains in the *bulk* of the sample. The coexisting domains of different polarizations are separated by a domain wall of highly frustrated holes.
In contrast, for ll-row confinement, the *entire* sample is x-polarized, and the polarization is strongest at the edges of the sample, in agreement with the framework presented in Fig. 5.1. Now the boundary holes will be the last holes to change (discontinuously) their polarization when increasing vertical compression. Confining a 9×10 sample on ll-rows, causes stress jumps in the S-curve for large vertical strains that coincides with the (dis)appearance of a small region of frustration near the *boundary* of the sample.

5.3 Homogenous confinement of large biholar systems

In this section we describe the mechanics, resulting from uniaxial loading, of two large biholar systems with homogenous horizontal boundary conditions. We first focus on a biholar system with 9×10 holes. In this system, the boundaries for even and odd rows differ as they start and end on both sides with large (ll-rows) or small holes (ss-rows). Secondly, we focus on a biholar sample with 8×10 holes. In this system, the boundaries for even and odd rows are similar but mirrored since each row either starts or ends with a large and small hole (ls- or sl-rows). For each system we apply three types of homogenous boundary conditions: (a) we clamp all the rows, (b) we clamp all even rows and (c) we clamp all odd rows. Then, for each of these types of confinements, a single $S(\varepsilon_y)$-curve is described in more detail.

5.3.1 9×10 holes

Shown in Fig. 5.5 are the $S(\varepsilon_y)$-curves for a 9×10 biholar sample ($\chi = 0.3$, $t = 0.15$ with $D_1 = 10$ mm, $D_2 = 7$ mm, $p = 10$ mm and d = 35 mm) with the three aforementioned clamping patterns (white arrows indicate the position of the transparent clamps). For each of these configurations we have increased the horizontal confinement ε_x, ranging from $\varepsilon_x = 0.00$ to $\varepsilon_x = 0.20$, and measured the mechanical response resulting from a vertical compression. Highlighted in red in Fig. 5.5 are a series of curves that will be discussed in more detail in the second part of this section.
In Fig. 5.5(a) all rows are clamped. For $\varepsilon_x < 0.04$ the $S(\varepsilon_y)$-curves are monotonic. For increasing values of ε_x, almost all curves show small non-monotonic and/or hysteretic regimes (best visible for $\varepsilon_x = 0.05$), however, not a clear trend is visible as a function of lateral confinement.
In contrast, the curves in Fig. 5.5(b), clearly show the four different mechanical regimes discussed in the previous chapters; (i) monotonic for $\varepsilon_x < 0.06$, (ii) non-monotonic for $0.06 \leq \varepsilon_x \leq 0.07$, (iii) hysteretic for $0.07 < \varepsilon_x < 0.18$, and (iv) a second monotonic regime for $\varepsilon_x > 0.19$. Moreover, for $0.10 < \varepsilon_x < 0.17$, the hysteretic jump during compression appears in two steps, first a large decrease in stress followed by an additional smaller jump. We observe similar behavior when decompressing the system, albeit it in reverse order: first a small increase in the stress followed by a large increase in stress. For values of $0.13 < \varepsilon_x < 0.17$, a

small third step is visible just before the last jump. Hence, in the hysteretic regime (iii), a large 9×10 system the $S(\varepsilon_y)$-curves display more structure compared to a small 5×5 laterally confined biholar sample.

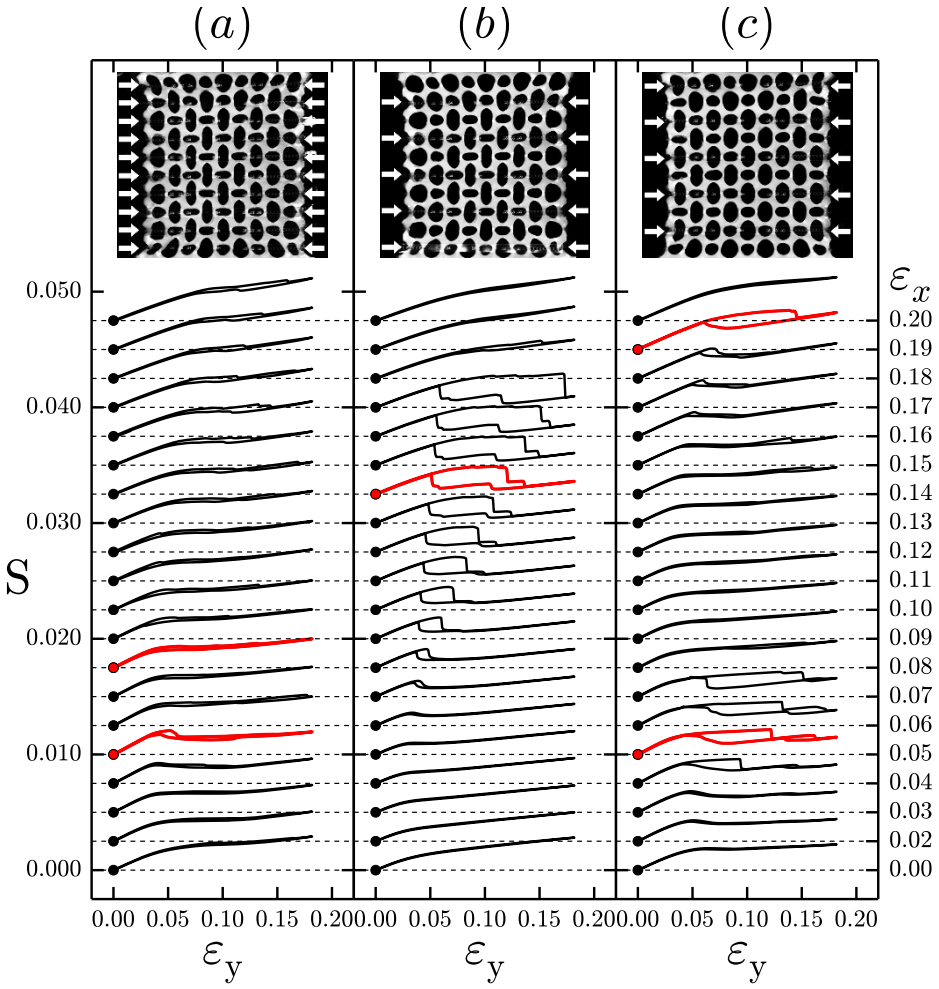

FIGURE 5.5: $S(\varepsilon_y)$-curves for a biholar sample ($\chi = 0.3$, $t = 0.15$) with 9×10 holes and three different ways of homogenous confinement (see insets) for a range of increasing confining strains. Curves are offset for clarity. (a) All rows of the sample are clamped. (b) All *ss*-rows are clamped. (c) All *ll*-rows are clamped. Highlighted in red are curves that are discussed in more detail in the text.

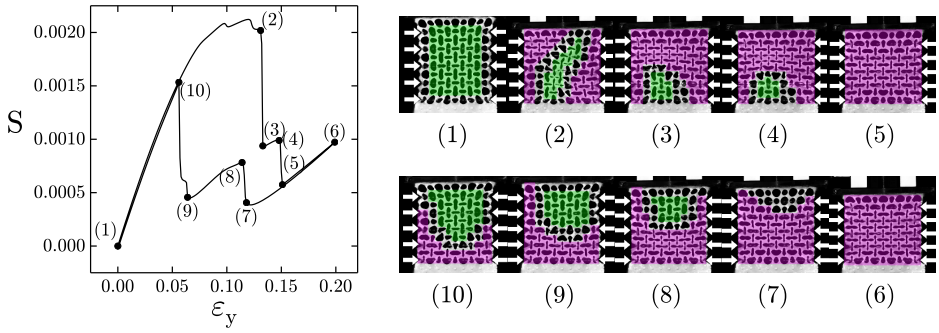

FIGURE 5.6: $S(\varepsilon_y)$-curve for a biholar sample ($\chi = 0.3$, $t = 0.15$) of 9×10 holes where all *ss*-rows are confined by $\varepsilon_x = 0.14$. Indicated in the curve are 10 points, corresponding to the 10 images on the right. The colors show the polarization of the domains, green for x-polarized and purple for y-polarized. White arrows indicate the location of the (transparent) clamps.

Shown in Fig. 5.5(c) are the $S(\varepsilon_y)$-curves for a 9×10 hole biholar sample with all *ll*-rows confined, for a range of strains ε_x. At $\varepsilon_x = 0.00$ the $S(\varepsilon_y)$-curve already shows some non-monotonic behavior, which enlarges for increasing confinement. For $0.03 < \varepsilon_x < 0.09$ we observe increasing hysteretic behavior with increasing lateral confinement. Moreover, we distinguish a small, but increasing, second hysteretic loop for higher values of ε_y. Increasing lateral confinement results in a series of monotonic force curves, up to $\varepsilon_x \approx 0.14$. Then, from $\varepsilon_x > 0.16$ a clear second hysteretic regime is visible whose strain range increases with lateral confinement and disappears at $\varepsilon_x > 0.20$.
To summarize, different clamping configurations show different mechanical responses and also different trends in mechanical responses as a function of confinement. Confining all rows in a 9×10 biholar sample leads to mainly monotonic $S(\varepsilon_y)$-curves with little hysteresis or structure. Clamping all *ss*-rows results in a series of $S(\varepsilon_y)$-curves showing the monotonic to non-monotonic to hysteretic transition scenario similar to 5×5 samples discussed before (Chapter 2 and 3). Finally, confining all *ll*-rows gives rise to a more complicated scenario with two regions of hysteretic behavior. In the following we discuss a series of $S(\varepsilon_y)$-curves (highlighted in red) in more detail, focusing on curves demonstrating hysteretic behavior.

Shown in Fig. 5.6 is the $S(\varepsilon_y)$-curve for the biholar sample confined on all *ss*-rows by $\varepsilon_x = 0.14$ (red curve in Fig. 5.5(b)). Indicated in the curve are 10 points with their corresponding images on the right. The colored regions, drawn by hand, indicate the polarization of the domains, green for x-polarized, purple for y-polarized. White arrows point the locations of the clamps. At the start of the experiment (1), the entire sample is x-polarized, except the boundary holes. Note that the polarization is strongest at the center of the sample. Arriving at (2), the sample is divided into three domains of different polarization. Two domains at the lateral boundaries are y-polarized, and a large domain in the bulk remains y-polarized. These domains are separated by a domain wall not thicker than a single hole. At (3), a large part of the x-polarized region in (2) has changed polarization and both separated y-polarized domains have joined to form a single y-polarized domain, corresponding to a jump in the $S(\varepsilon_y)$-curve. The entire sample is now divided into two domains separated by a domain wall. This first jump in stress is followed by a second rapid decrease in stress between (4)-(5). Arriving at (4), the y-polarized domain has smoothly decreased in size. Between (4)-(5), this small y-polarized domain has rapidly changed polarization and the sample is now entirely y-polarized at (5). Decompressing the sample, from (6) to (10), we observe a growing x-polarized domain in the bulk of the sample where a sudden change in polarization of a domain in the sample results in a peak rapid increase of the stress in the $S(\varepsilon_y)$-curve.
We conclude that confining the 9×10 biholar sample on all *ss*-rows, at large enough confinements, results in a hysteretic loop where the structure in the $S(\varepsilon_y)$-curve are a result of instantaneous changes in polarizations of large domains in the bulk of the material. In agreement with the framework presented in Fig. 5.1, initially the polarization is a function of x, and is strongest in the bulk of the sample, which therefore needs the highest vertical compressions to change polarization.

Shown in Fig. 5.7 is the $S(\varepsilon_y)$-curve for the biholar sample confined on the odd rows by $\varepsilon_x = 0.05$ (lowest red curve in Fig. 5.5(c)). Indicated in the curve are 6 points with their corresponding images on the right, with the green and purple colors marking the polarization of the sample. At (1) the sample is fully x-polarized and is strongest polarized at the lateral boundaries of the sample. Increasing the applied strain, the sample

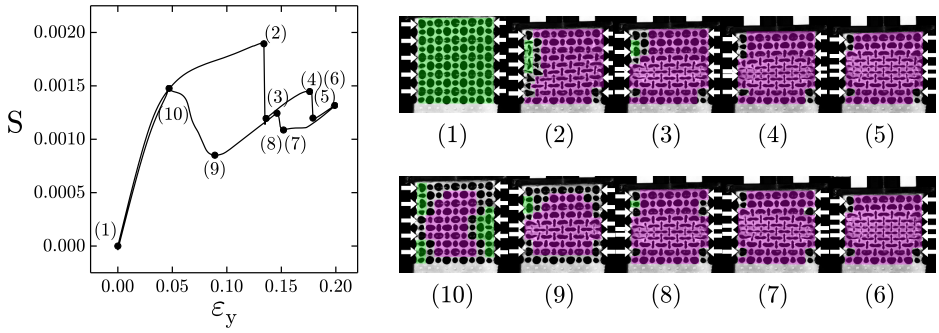

FIGURE 5.7: $S(\varepsilon_y)$-curve for a biholar sample ($\chi = 0.3$, $t = 0.15$) of 9×10 holes where all *ss*-rows are confined by $\varepsilon_x = 0.05$. Indicated in the curve are 10 points, corresponding to the 10 images on the right. The colors show the polarization of the domains, green for x-polarized and purple for y-polarized. White arrows indicate the location of the (transparent) clamps.

smoothly changes the polarization, except for a small domain on the left lateral boundary of the sample. The jump between (2)-(3) is caused by an event at the *boundary* of the sample. As before, the central clamp gets misaligned. The second jump in stress between (4) and (5) is caused by a similar event near the second clamp from the top.
The peaks in the $S(\varepsilon_y)$-curve for decompressing the sample are resulting from similar events. Finally, at (10), there are x-polarized regions along the lateral boundaries, while in the center of the sample there exist a large region of y-polarized holes, which smoothly changes polarization when decompressing further.
We conclude that for this configuration of clamps there are no large domains in the bulk of the sample with different polarizations. In agreement with the framework presented earlier, initially the entire sample is x-polarized, with the polarization strongest at the lateral boundaries. Compressing the system vertically will change the polarization of the sample to y, starting from the weakest x-polarized regions. The hysteresis in the $S(\varepsilon_y)$-curve for $0.04 < \varepsilon_x < 0.09$ is due to events occurring at the boundary of the sample.

Shown in Fig. 5.8 is the $S(\varepsilon_y)$-curve for the biholar sample confined on all *ll*-rows by a larger amount ($\varepsilon_x = 0.19$) (top red curve in Fig. 5.5(c)). For

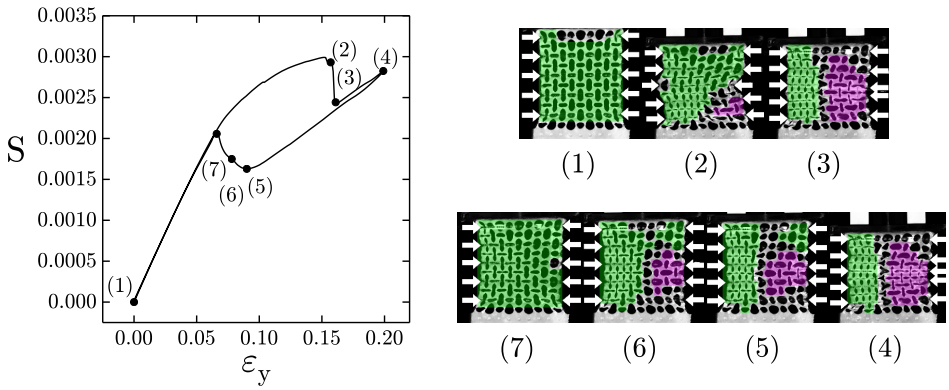

FIGURE 5.8: $S(\varepsilon_y)$-curve for a biholar sample ($\chi = 0.3$, $t = 0.15$) of 9×10 holes where all *ss*-rows are confined by $\varepsilon_x = 0.19$. Indicated in the curve are 7 points, corresponding to the 7 images on the right. The colors show the polarization of the domains, green for x-polarized and purple for y-polarized. White arrows indicate the location of the (transparent) clamps.

small compression the sample is entirely x-polarized, with the polarization strongest at the lateral edges of the sample. However, in contrast to the curve for $\varepsilon_x = 0.05$, at the top of the peak (2), a large domain remains x-polarized. Only a small region in the bottom right of the sample has changed polarization. At (3), the sample shows two domains of opposite polarization, separated by a domain wall. The left side of the sample is x-polarized while the right side of the sample is y-polarized. Note that the right part of the central clamp has jumped downward. Hence, between (2)- (3) an event at the boundary triggered a rapid change of polarization in the bulk of the material. Decompressing the sample we observe a less extreme pattern transformation. From (5)-(7) the x-polarized domain is smoothly expanding towards the right side of the sample until, at (7), the entire sample is x-polarized.

We conclude that for a biholar 9×10 biholar sample, if all *ll*-rows (rows starting and ending with a big hole) are confined we can distinguish two different scenarios as a function of confinement. For low confinements, $\varepsilon_x < 0.08$, we observe a non-monotonic to hysteretic transition in the $S(\varepsilon_y)$-curves. The hysteretic jumps in the $S(\varepsilon_y)$-curves are caused by iso-

lated events at the boundary of the sample, as the initial x-polarization is strongest here. For high confinements, $\varepsilon_x \geq 0.08$, the sample is separated into two domains of different polarization and a large region of highly frustrated holes. A single event at the boundary of the sample triggers a large pattern transformation in the bulk of the material, leading to a large region of frustrated holes.
Shown in Fig. 5.9 is the $S(\varepsilon_y)$-curve for a biholar sample confined on *all* rows with $\varepsilon_x = 0.05$ (red curve in Fig. 5.5(a)). At (1) the sample is x-polarized, and as expected, the polarization is strongest at the lateral boundaries of the sample. Then at (2), the maximum of the $S(\varepsilon_y)$-curve, two y-polarized domains have smoothly emerged, without notable events in the $S(\varepsilon_y)$-curve, at opposite boundaries of the sample: one at the upper left side and one at the lower right side of the sample. When the compression is further increased, the stress jumps down, and the pattern changes discontinuously. At (3), there is only one y-polarized domain, running from top left to bottom right which separates two x-polarized domains at the top right and bottom left. Hence, the jump in stress between (2) and (3) is a result of a change in polarization of a large region in the bulk of the sample. At (4) the entire system is y-polarized, except small regions at the boundary of the sample, where holes are almost triangular shaped. Notice that clamps in the center of the sample are skewed – on the left side the some clamps collide while on the right side the distance between the central clamps increased. When lowering the strain, between (5) and (6) a small region in the top left of the sample discontinuously changed polarization from y- to x, resulting in a small decrease in stress when decompressing. Between (6) and (7) the x-polarized domain smoothly grows to span three-quarter of the system size, resulting in a smooth increase in the stress when decompressing the sample. Decreasing the strain further, the pattern smoothly evolves to a pure x-polarized state at zero strain.

A more typical $S(\varepsilon_y)$-curve for 9×10 biholar sample with all the rows are confined is presented in Fig. 5.10 ($\varepsilon_y = 0.08$). Although there is structure and hysteresis in the $S(\varepsilon_y)$-curve there are no large jumps in stress as shown in Fig. 5.9. At (1) the sample is x-polarized and is strongest in the bulk of the sample. Then at (2), a local maximum of the $S(\varepsilon_y)$-curve, two domains of different polarization, separated by a vertical domain wall, running from top to bottom, have smoothly emerged. When the com-

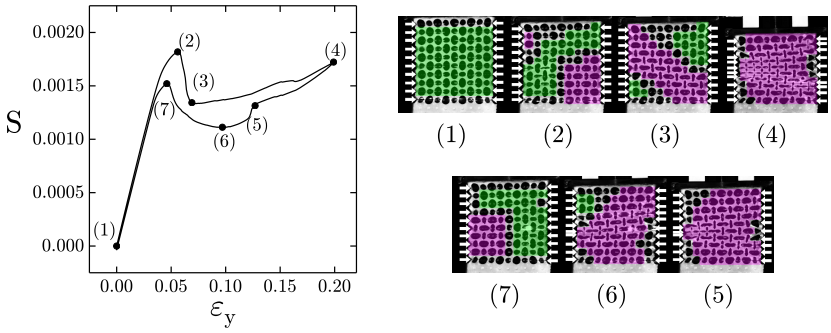

FIGURE 5.9: $S(\varepsilon_y)$-curve for a biholar sample ($\chi = 0.3$, $t = 0.15$) of 9×10 holes where all rows are confined by $\varepsilon_x = 0.05$. Indicated in the curve are 7 points, corresponding to the 7 images on the right. The colors show the polarization of the domains, green for x-polarized and purple for y-polarized. White arrows indicate the location of the (transparent) clamps.

pression is further increased, at (3), the y-polarized domain has slightly expanded discontinuously at the bottom half of the sample, forcing the domain wall to move in the left direction, causing a small jump in the $S(\varepsilon_y)$-curve. A similar event, now at the top half of the sample, is occurring between (4) and (5), resulting in a tiny jump in the $S(\varepsilon_y)$-curve. At 6 the sample is divided into two domains, a small x-polarized domain on the left side of the sample, running from top to bottom, and a large y-polarized domain spanning the other part of the sample. The two domains are separated by a straight vertical domain wall. Lowering the strain from (6) to (7), the x-polarized domain smoothly expands from left to right until both x- and y-polarized domains are of comparable size at (7). Decreasing the strain further, the pattern smoothly evolves to a pure x-polarized state at zero strain.

To conclude, when confining all holes of a 9×10 biholar sample, the jumps in the $S(\varepsilon_y)$-curve can be connected to domains discontinuously changing polarization in the bulk of the sample. A small disturbance of the symmetries in the system, by position the pins that confine the sample not exactly at the center of the holes or slightly skewed top and bottom plate, causes the domains walls to grow from the right (Fig. 5.10) or left during compression, or from both directions (Fig. 5.9). Initially, the polarization is strongest in the center of the sample, therefore polarization changing

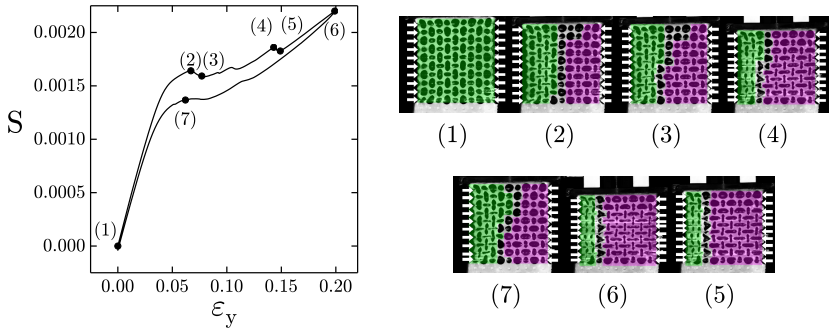

FIGURE 5.10: $S(\varepsilon_y)$-curve for a biholar sample ($\chi = 0.3$, $t = 0.15$) of 9×10 holes where all rows are confined by $\varepsilon_x = 0.08$. Indicated in the curve are 7 points, corresponding to the 7 images on the right. The colors show the polarization of the domains, green for x-polarized and purple for y-polarized. White arrows indicate the location of the (transparent) clamps.

events will take place in the bulk of the sample, not at the boundaries.

5.3.2 8×10 holes

In this section we study the mechanical response resulting from uniaxial loading a 8×10 biholar sample with $\chi = 0.3$ and $t = 0.15$ ($D_1 = 10$ mm, $D_2 = 7$ mm, $p = 10$ mm, $d = 35$ mm) for the three aforementioned configurations of confinement. With 8 holes in the horizontal direction, the dimensionless stress S is defined as:

$$S := \frac{\sigma_y}{E} \frac{A_{\text{eff}}}{A} = \frac{9t'F}{dE(L_x + 2t')^2}\,, \tag{5.3}$$

where the width of the top row is given by $L_x = 8p + D_1/2 + D_2/2$. For an even number of columns, the distance between the metal rods without clamps L_{c0} is the same for each row, and in the case of 8×10 sample, reads: $L_{c0} = 9p - D_2/2 - D_1/2 = 81.5$ mm. Moreover, we refer to rows starting with a large (small) hole and ending with a small (large) hole as ls-rows (sl-rows).

Shown in Fig. 5.11 are the $S(\varepsilon_y)$-curves for the 8×10 biholar sample with the three clamping patterns (white arrows indicate the position of the transparent clamps). For each of these configurations we have increased the horizontal confinement ε_x, ranging from $\varepsilon_x = 0.00$ to $\varepsilon_x = 0.20$. Highlighted in red are a series of curves that will be discussed in more detail in the second part of this section.
All three series of $S(\varepsilon_y)$-curves for the different clamping configurations, Fig. 5.11(a)-(c), display the monotonic to non-monotonic to hysteretic scenario similar to the 5×5 samples discussed before (chapters 2 and 4). Note that in Fig. 5.11(b) and Fig. 5.11(c), where in both cases five clamps are used to confine the sample, the sequence of curves are quite similar due to the $x \leftrightarrow -x$ symmetry that relates these experiments. In Fig. 5.11(a), where 10 clamps are used to confine the sample, the different transitions are more concentrated in a smaller range of ε_x. At high values of confinement, $\varepsilon_x \geq 0.15$, a second hysteretic regime is visible.
To summarize, the different clamping configurations *do not* show different trends in mechanical responses for a 8×10 biholar sample; in all three cases ((a) all rows confined, (b) all *ls*-rows confined, (c) all *sl*-rows confined) the monotonic to non-monotonic to hysteretic scenario is present. Moreover, the values of confinement are very similar for confining all *ls*-rows and *sl*-rows. Confining all rows of the 8×10 biholar sample show a second hysteretic regime, where the hysteretic loop is increasing as a function of confinement as well. Although the mechanical responses are similar, in the following we will show that the change in (domains of) polarization is strongly dependent on the clamping configuration. Curves highlighted in red will be discussed in more detail below.

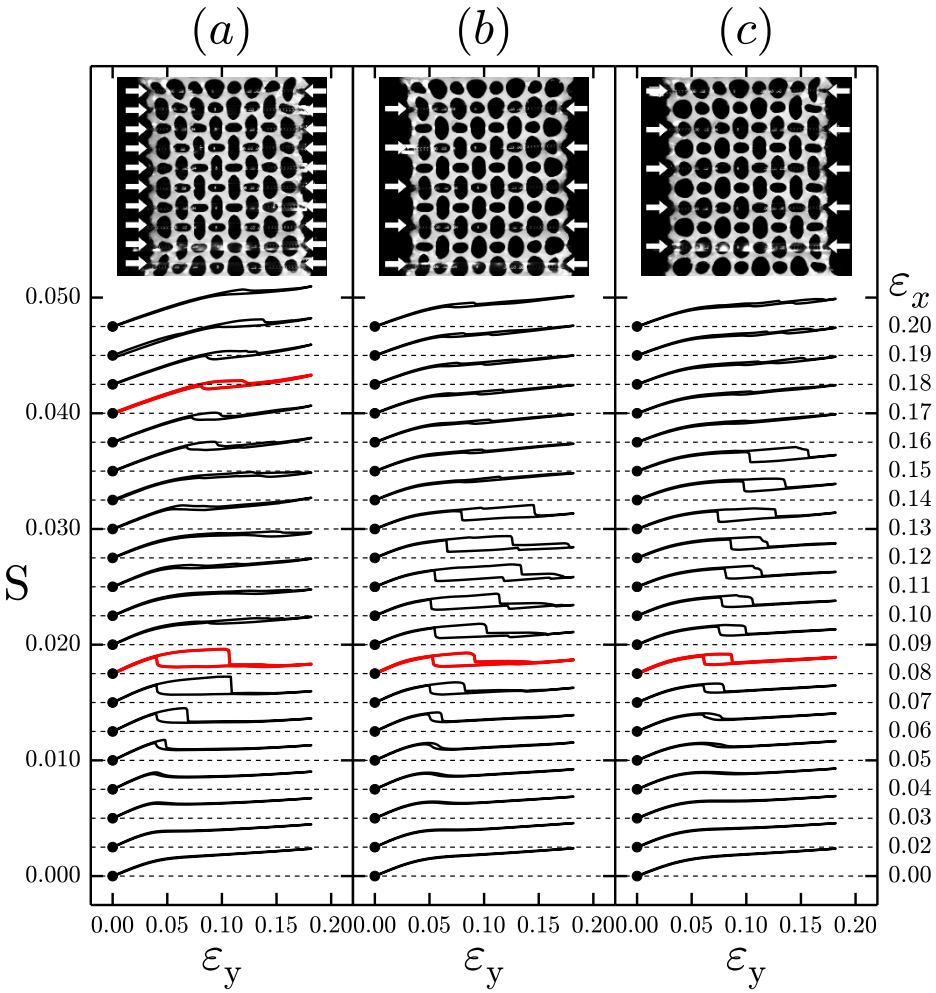

FIGURE 5.11: $S(\varepsilon_y)$-curves for a biholar sample ($\chi = 0.3$, $t = 0.15$) with 8×10 holes and three different ways of homogenous confinement (see insets) for a range of increasing confining strains. Curves are offset for clarity. (a) All rows of the sample are clamped. (b) All *ls*-rows are clamped. (c) All *sl*-rows are clamped. Highlighted in red are curves that are discussed in more detail in the text. For (b) and (c) the values of confinement ε_x for the different transitions are very comparable; monotonic for $0.00 \leq \varepsilon_x \leq 0.02$ in (b) and $0.00 \leq \varepsilon_x \leq 0.03$ in (c), non-monotonic for $0.03 \leq \varepsilon_x \leq 0.05$ in (b) and $0.04 \leq \varepsilon_x \leq 0.06$, hysteretic for $0.06 \leq \varepsilon_x \leq 0.13$ in (b) and $0.07 \leq \varepsilon_x \leq 0.15$ and overall monotonic with a small amount of structure for $\varepsilon_x \geq 0.14$ in (b) and $\varepsilon_x \geq 0.16$. In (a) the values of confinement ε_x for the different transitions are concentrated in a smaller range of ε_x; monotonic for $0.00 \leq \varepsilon_x \leq 0.02$, non-monotonic for $0.03 \leq \varepsilon_x \leq 0.04$, and hysteretic for $0.05 \leq \varepsilon_x \leq 0.08$.

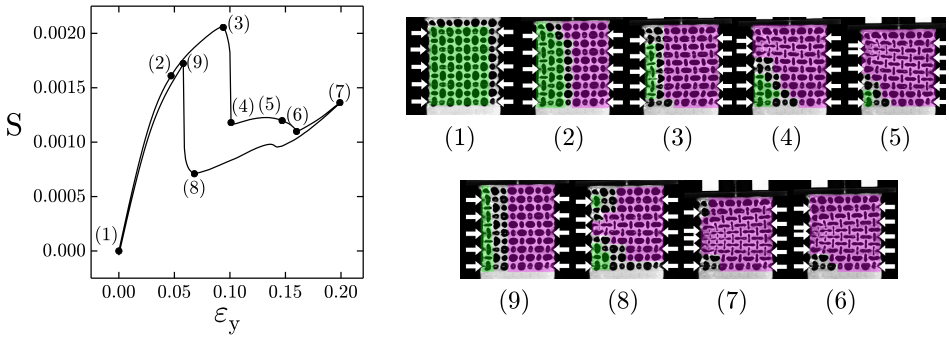

FIGURE 5.12: $S(\varepsilon_y)$-curve for a biholar sample ($\chi = 0.3$, $t = 0.15$) of 8×10 holes where all ls-rows are confined by $\varepsilon_x = 0.08$. Indicated in the curve are 9 points, corresponding to the 9 images on the right. The colors show the polarization of the domains, green for x-polarized and purple for y-polarized. White arrows indicate the location of the (transparent) clamps.

Shown in Fig. 5.12 is the $S(\varepsilon_y)$-curve for the 8×10 biholar sample with all ls-rows confined by $\varepsilon_x = 0.08$ (red curve in Fig. 5.11(b)). Indicated in the curve are 9 points with their corresponding images on the right, with the green and purple colors marking the polarization of the (domains of the) sample. The $S(\varepsilon_y)$-curve shows a large jump in stress between (3) and (4), followed by a smaller decrease in stress between (5) and (6). At (1) the sample is x-polarized. A gradient in polarization is visible from left (strongly x-polarized), where all the l-holes are confined, to right (weakly x-polarized), where all the s-holes are confine – again, this is consistent with our scenario. Arriving at (3), via (2), by increasing the strain, a y-polarized domain is smoothly expanding from the *right side* of the sample, growing towards the region that initially is strongest x-polarized, dividing the sample in two domains separated by a domain wall. Going from (3) to (4), the pattern discontinuously changes, and at (4) the sample is y-polarized, except for a small triangular shaped region in the bottom left side of the sample. Note that the top two clamps, indicated by the arrows, are skewed. The jump is stress between (3) and (4) is due to a rapid change in polarization of a couple of holes in the top left of the sample, initiated by the snapping of a beam at the left lateral boundary between the first two clamps. The second large dip in stress between (5) and (6) is due to a similar snapping event of the left lateral boundary beam between clamp

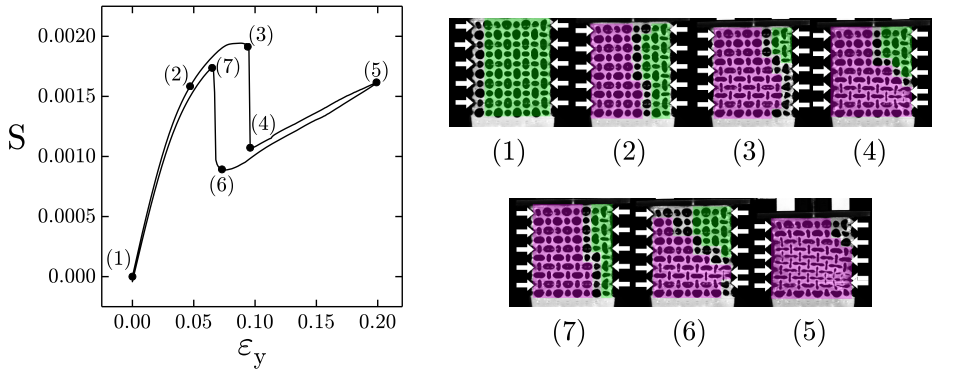

FIGURE 5.13: $S(\varepsilon_y)$-curve for a biholar sample ($\chi = 0.3$, $t = 0.15$) of 8×10 holes where all *sl*-rows are confined by $\varepsilon_x = 0.08$. Indicated in the curve are 6 points, corresponding to the 6 images on the right. The colors show the polarization of the domains, green for x-polarized and purple for y-polarized. White arrows indicate the location of the (transparent) clamps.

2 and 3. At (7) the sample is strongly y-polarized. Decreasing the strain, at (8) there are two small regions of x-polarization on the left side of the system, separated by a large y-polarized region. At (9), the system is split into two domains, a y-polarized domain and x-polarized domain at the left boundary of the sample, separated by a vertical boundary wall. The rapid increase between (8) and (9) is due to the change in curvature of the left boundary beam between the second and third clamp, and the concomitant discontinuous change in polarization. Hence, most of the pattern changes reflect the top-down symmetry and the broken left-right symmetry of the system, following the gradient in initial polarization (from left to right), in agreement with the framework presented in section 5.1.

Shown in Fig. 5.13 is the $S(\varepsilon_y)$-curve for the 8×10 biholar sample with all *sl*-rows confined by $\varepsilon_x = 0.08$ (red curve in Fig. 5.11(c)). This situation is the mirror image of the situation shown in Fig. 5.12, although many details differ. At (1) the system is x-polarized. Now the gradient in polarization runs from right (strongly x-polarized) to left (weakly x-polarized). Arriving at (3), via (2), by increasing the strain, a y-polarized domain is smoothly expanding from the *left side* of the sample. The vertical domain wall, separating the two regions of different polarizations, travels horizon-

tally from left to right through the sample as a function of applied vertical strain,towards the region of strong x-polarization. At (3), only a small region in the top right of the sample is x-polarized. Moreover, part of the domain wall has reached the right boundary of the system, resulting in a series of highly frustrated triangular shaped boundary holes. By slightly increasing the compressive strain, at (4), the y-polarized region has expanded, at the bottom half of the sample, towards the right boundary of the sample. The fourth clamp from the top is skewed. Note that the x-polarized region in the top right of the sample also expanded slightly. The jump is stress between (3) and (4) is due to a beam snapping event on the right side of the sample, between clamps four and five from the top. At (5), the entire sample is y-polarized, except a small region of frustrated holes at the top right of the sample. Between (5) and (6) this frustrated region becomes x-polarized and is growing in size. At (7), the entire right side of the sample is x-polarized. The jump between (6) and (7) is a result of a rapid change in polarization of boundary holes at the right edge of the sample.
To conclude, the hysteretic jumps in the $S(\varepsilon_y)$-curves for confining all ls-rows or all sl-rows of a 8×10 biholar sample are resulting from events at the boundary of the system and the concomitant discontinuous changes of the polarization in the bulk. By changing the boundary conditions between "all ls-rows" or "all sl-rows", we can control the flow of the domain wall during compression of the biholar sample as the initial gradient in polarization is set by the configuration of the clamps and runs from l-confined boundary holes (strongly x-polarized) to s-confined boundary holes (weakly x-polarized). When all ls-rows are confined, a vertical domain wall separating a x-polarized and a y-polarized region is traveling from the *left* side *to* the *right* side of the sample. By confining all sl-rows, the vertical domain wall is moving from the *right* side *to* the *left* side of the sample. When the domain wall hits one of the lateral boundaries, a beam of one of its highly frustrated holes snaps, causes a pattern transformation and resulting in a jump in stress.

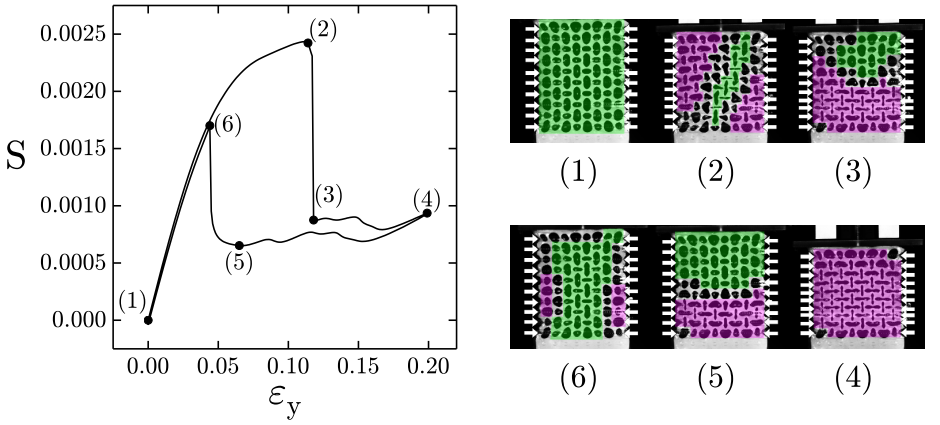

FIGURE 5.14: $S(\varepsilon_y)$-curve for a biholar sample ($\chi = 0.3$, $t = 0.15$) of 8×10 holes where all rows are confined by $\varepsilon_x = 0.08$. Indicated in the curve are 6 points, corresponding to the 6 images on the right. The colors show the polarization of the domains, green for x-polarized and purple for y-polarized. White arrows indicate the location of the (transparent) clamps.

Now the question arises what will happen when all rows are confined and the system is left-right symmetric. Shown in Fig. 5.14 is the $S(\varepsilon_y)$-curve for the 8×10 biholar sample with *all* rows confined by $\varepsilon_x = 0.08$ (first red curve in Fig. 5.11(a)). At (1) the system in x-polarized, but now the polarization is strongest in the bulk of the sample. At (2) the system is split into three domains: a x-polarized regions running diagonally through the system sandwiched by two triangular shaped y-polarized domains at the top left side and the bottom right side of the sample. The three regions are separated by two boundary walls consisting of highly frustrated holes. Slightly increasing the applied vertical strain results in a sample, at (3), that is split into two large domains: a x-polarized region at the top half of the system and a y-polarized domain at the bottom half of the system. The jump between (2) and (3) is a result of a rapid pattern transformation in the bulk of the sample. At (4) the sample is entirely y-polarized. Between (4) and (5) a x-polarized region is expanding from the top of the sample. At (6), the system is split into three regions of different polarization: a large x-polarized system occupying almost the entire sample and two y-polarized domains at the lateral boundaries of the sample. Hence, the jump between

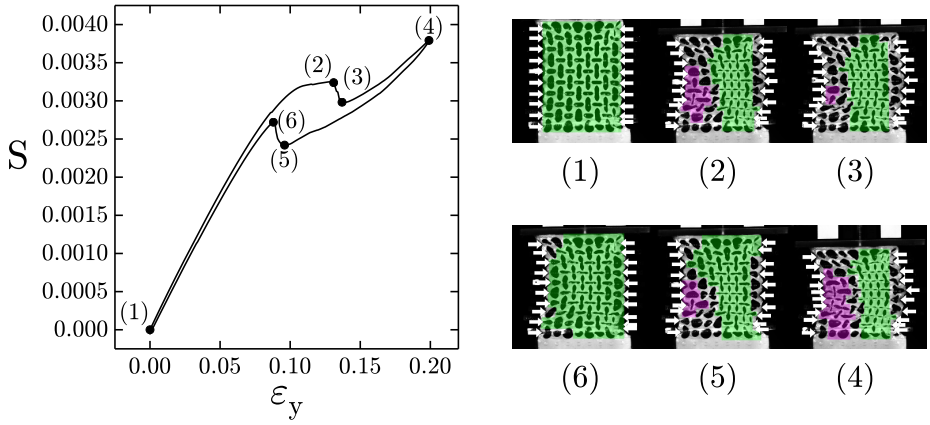

FIGURE 5.15: $S(\varepsilon_y)$-curve for a biholar sample ($\chi = 0.3$, $t = 0.15$) of 8×10 holes where all rows are confined by $\varepsilon_x = 0.17$. Indicated in the curve are 6 points, corresponding to the 6 images on the right. The colors show the polarization of the domains, green for x-polarized and purple for y-polarized. White arrows indicate the location of the (transparent) clamps.

(5) and (6) is the result of a large change in polarization in the bulk of the sample. However, we see that the polarization patters remain close to the left-right symmetric.

Shown in Fig. 5.15 is the $S(\varepsilon_y)$-curve for the 8×10 biholar sample with all rows confined by a much larger strain, $\varepsilon_x = 0.17$ (second red curve in Fig. 5.11(a)). At (1) the system in x-polarized, with the polarization being strongest in the bulk of the sample. At (2) a small y-polarized region appeared on the left side of the system and large parts of both lateral boundaries of the system are highly frustrated. At (3), this small region has become smaller. Moreover, the entire sample has buckled, breaking the left-right symmetry globally. The jump in stress between (2) and (3) is due to this global buckling of the sample. At (4), the y-polarized domain in the buckled sample has grown. Decompressing the system to (5), shows that the x-polarized domain has expanded and the y-polarized domain has become smaller. Furthermore, the sample is less buckled. At 6, the sample is not buckled anymore and the entire system is x-polarized, except individual holes that are frustrated. The sudden increase in stress between 5 and 6 is due to the unbuckling of the whole sample with related

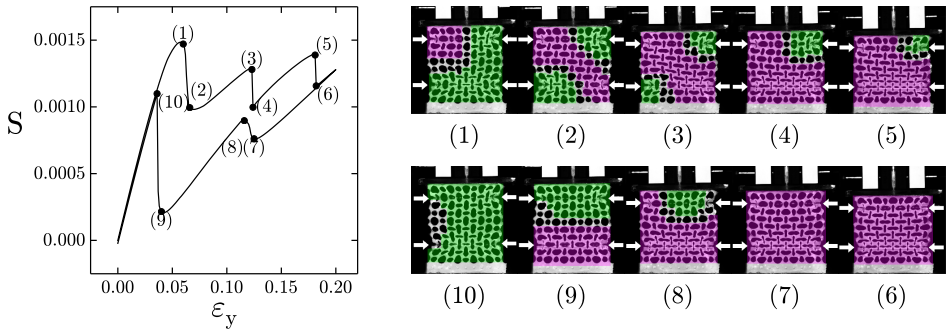

FIGURE 5.16: $S(\varepsilon_y)$-curve for a biholar sample ($\chi = 0.3$, $t = 0.15$) of 9×10 holes where two *ss*-rows, row 2 and 8, are confined with $\varepsilon_x = 0.21$. Indicated in the curve are 10 points, corresponding to the 10 images on the right. The colors show the polarization of the domains, green for x-polarized and purple for y-polarized. White arrows indicate the location of the (transparent) clamps.

polarization change at the boundary.
To conclude, the hysteretic jumps in the $S(\varepsilon_y)$-curves for confining all rows of a 8×10 biholar sample are, for $\varepsilon_x < 0.09$, resulting from a rapid pattern transformation in the bulk of the sample, as the initial x-polarization is strongest in this region. By confining all rows, the domain wall already present for *ls*-confinement, traveling from left to right, and the domain wall already present for *sl*-confinement, traveling from right to left, are on the verge of colliding at the peak of the $S(\varepsilon_y)$-curve. The hysteretic jumps in the $S(\varepsilon_y)$-curves for high values of confinement, $\varepsilon_x \leq 0.09$, are resulting from global buckling of the entire sample, with accompanying change in polarization of small regions of the sample. The combined effect of global buckling and local pattern transformation is beyond the study presented in this thesis.

5.4 Controlling the domain walls

As discussed in the previous section, by changing the boundary conditions (barcode) of a 8×10 biholar sample it is possible to control direction of propagation of an emerging domain wall. In this section we will study two ways of programming the mechanical response by programming an

(emerging) domain wall in a 9×10 and a 9×11 biholar sample.
Depicted in Fig. 5.16 is the $S(\varepsilon_y)$-curve for the 9×10 biholar sample with two *ss*-rows (rows 2 and 8) confined by $\varepsilon_x = 0.21$. For compression the $S(\varepsilon_y)$-curve shows three peaks, while for decompression the curve shows two clear jumps. Indicated in the curve are 10 points, with the corresponding images right. At the start, the image is entirely x-polarized, except the small regions near the boundaries of the clamps (not shown here). Then, arriving at the first peak, (1), the top left quadrant of the sample has smoothly changed polarization. At (2), the y-polarized domain runs diagonally through the sample, from top left to bottom right, leaving two domains x-polarized at the top right and left bottom. The jump between (1) and (2) is caused by a large, discontinuous change in polarization in the bulk of the sample. Next, between (3) and (4) the x-polarized domain in the bottom left of the sample, present in (3), has changed polarization at (4). The last jump in the curve between (5) and (6), is due to a change of polarization of a x-polarized domain at the top right of the sample. At (6) and (7) the sample is fully y-polarized. In the decompression part of the curve we observe a different scenario from the compression sweep. First, between (7) and (8) a large region at the top of the sample changes polarization, focused around the top clamp. And finally, between (9) and (10), the bottom part of the system changes polarization to x-polarized.
To summarize, by using two clamps on different *ss*-rows, we generate multiple peaks in the $S(\varepsilon_y)$ curve as a function of deformation. As only *ss*-rows are used to confine the sample, the structure in the curve is caused by the change of polarization of large domains in the bulk of the sample. The locations of the domains differ between compression and decompression.

To gain even more control over the propagation of domain walls through the sample, and thus over the compressive force, we apply a gradient in confinement, which will guide the domain wall from regions of low confinement to regions of high confinement as the sample is compressed. Shown in Fig. 5.17 is the $F(\varepsilon_y)$-curve of a 9×11 biholar sheet ($D_1 = 10$ mm, $D_2 = 7$ mm, $\chi = 0.3, t = 0.15$) subjected to uniaxial loading with a gradient in horizontal confinement on all *ss*-rows. We use five clamps of decreasing length as function of row number, corresponding to strains $\varepsilon_x = 0.08, 0.11, ..., 0.2$. As shown in Fig. 5.17(a), this results in a giant hys-

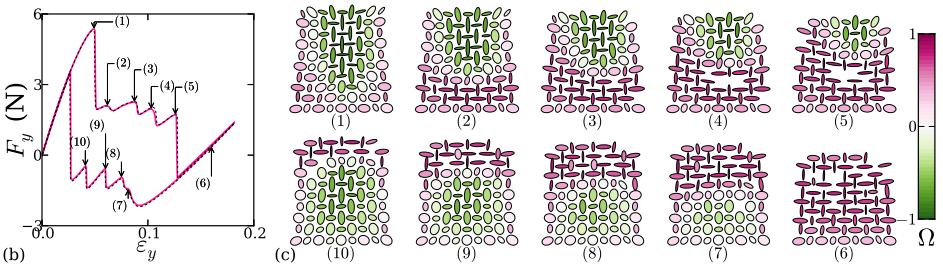

FIGURE 5.17: (a) Force-displacement curve for an inhomogeneously confined 9×11 system, showing two giant hysteresis loops with multiple, perfectly reproducible polarization switching events. (b) Snapshots of the state of our experimental metamaterial corresponding to (1)-(10), where color codes for polarization.

teresis loop with multiple peaks. We stress that Fig. 5.17(a) overlays two subsequent hysteretic loops, illustrating that this complex behavior is well reproducible. As shown in Fig. 5.17(b), each of these peaks corresponds to a polarization switch of part of the material. Under compression a domain wall travels from bottom to top through the sample, under decompression, a polarization wave travels from top to bottom through our material. We note that the spatial configurations in the downsweep of ε_y are not the same as in the upsweep, which can be understood from the observation that the most confined part of the system shows the most hysteresis.

5.5 Example of Barcode Programming

Shown in Fig. 5.18 is an example of the different $S(\varepsilon_y)$-curves that are obtained when two clamps are used to confine a 9×10 biholar sample ($\chi = 0.3$, $t = 0.15$) at 4 different configurations, or barcodes. Shown in Fig. 5.18(a) is the $S(\varepsilon_y)$-curve when two *ss*-rows, row 8 and row 2, are confined by $\varepsilon_x = 0.20$. We observe three peaks for compression and two peaks for decompression, similar to the $S(\varepsilon_y)$-curve shown Fig. 5.16.
When one *ss*-row and one *ll*-row are confined, a single peak is observed, Fig. 5.18(b) and (c). Note that the hysteresis loop for Fig. 5.18(c) is larger then Fig. 5.18(b). Both confined rows in Fig. 5.18(c) are further away from the fixed top and bottom boundaries than the confined rows in Fig. 5.18(b). This results in a larger hysteretic loop for two reasons: (*i*) The pattern in

Fig. 5.18(c) at the start of the run, is more homogenous and locally stronger x-polarized than the the pattern in Fig. 5.18(b). (*ii*) Around the confined *ss*-row in Fig. 5.18(c) there are more holes available in the bulk of the sample that are free to change polarization.
Confining two *ll*-rows, row 3 and 9, shows an almost monotonic $S(\varepsilon_y)$-curve with a very small hysteretic loop for high strains, $\varepsilon_y > 0.15$. The structure in the $S(\varepsilon_y)$-curve is due to a single snapping event at the boundary of the sample.
When using two clamps of same length, we obtain, depending on the position of the clamps, four qualitatively different mechanical responses from a single biholar sample. This shows that we can program the mechanical response with the location(s) of confinement. Hence, we succesfully created a barcode metamaterial where the mechanical response is programmed by the boundary conditions.

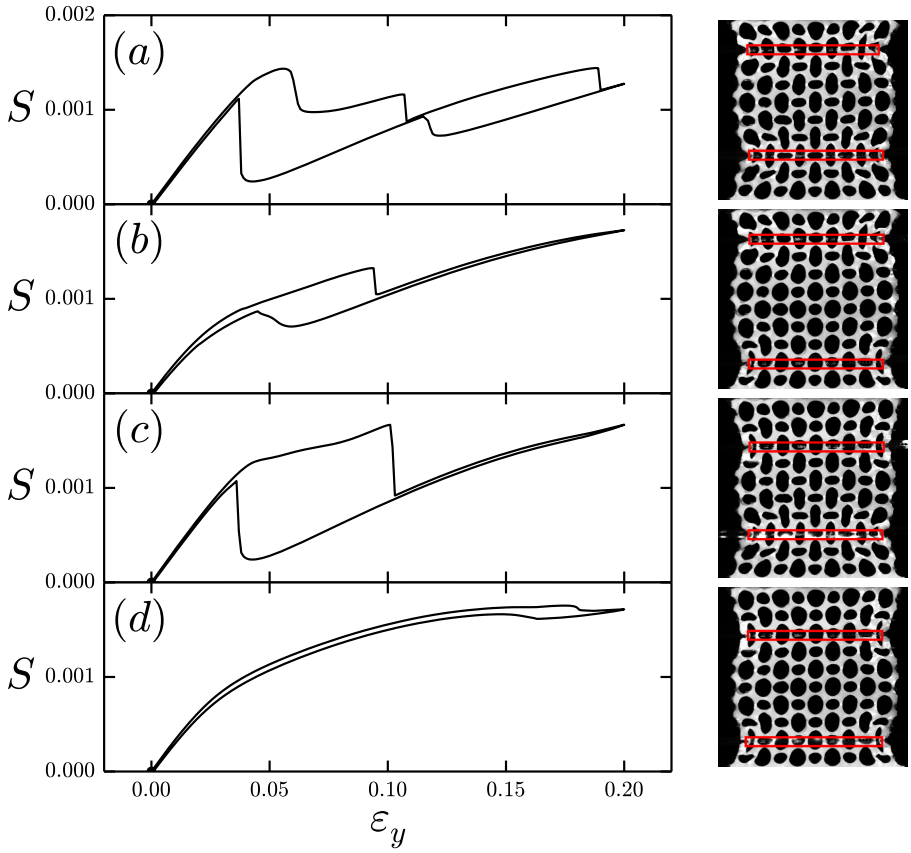

FIGURE 5.18: $S(\varepsilon_y)$-curves for a biholar sample ($\chi = 0.3$, $t = 0.15$) of 9×10 holes where four different configurations of two clamps, highlighted in red in the insets, are used to confine the sample by $\varepsilon_x = 0.20$. (a) Row 2 and row 8, both *ss*-rows, are confined. (b) Row 2 (*ss*-row) and row 9 (*ll*-row) are confined. (c) Row 3 (*ll*-row) and row 8 (*ss*-row) are confined. (d) Row 3 (*ll*-row) and row 9 (*ll*-row) are confined.

5.6 Conclusion

In this chapter we showed that inhomogeneities in the polarization field induced by the lateral clamps play an important role. After clamping but before compression, ($\varepsilon_y = 0$ and $\varepsilon_x > 0$), the bulk of biholar samples are x-polarized - this is the basic feature allowing programmability of the materials response under uniaxial compression. However, the polarization near the edges strongly depends on whether a small or large hole is clamped, and the resulting difference between edge and bulk sets up gradients in the polarization throughout the sample. Specifically, clamping a large boundary hole leads to a strong local x-polarization, larger than the bulk, leading to a gentle decay of the x polarization from edge to bulk. In contrast, clamping a small hole leads to a locally strong y-polarized region, setting up a strong gradient from y to x polarized states from edge to bulk.

This simple observation, which ultimately stems from the difference in x forcing in the bulk (compression along the horizontal beams) and near the boundary (bending of the vertical beams), and which can be rationalized by reconsidering our soft mechanism model, has a number of consequences. First, for samples with an odd number of columns, such as the 9×10 biholar samples studied here, horizontal clamps either confine ss- or ll-rows, where the maximally polarized region is either in the bulk or near the edge. For ss-clamping, the maximally polarized region is in the bulk, and compression first changes the polarization near the edge before affecting the bulk. Various smooth and discontinuous pattern transformations then occur in the bulk — depending on the amount of lateral confinement —following the bifurcation scenarios encountered before. In contrast, for ll-clamping, the maximally x-polarized region is at the edges, and under compression a domain wall between bulk y-polarization and edge x-polarization moves towards the edge. However, even for substantial compression, a tiny x-polarized defect gets trapped at the boundary, which may disappear in a highly localized discontinuous event leading to more complex behavior, very sensitive to, e.g., misalignment of the clamps or inhomogeneities of the sample causing the left and right boundaries of a single row to become out of sync.

Second, for a sample with an even number of columns, such as the 8×10 sample studied above, we can confine either ls- or sl-rows. As a conse-

quence, there is a gradient from strong x polarization to y-polarization along the horizontal coordinate of the samples. This leads to a vertical domain wall that propagates through the sample under compression, until it hits the boundary where a x-polarized defect is trapped, leading to a discontinuous pattern change under further compression.
Third, to obtain more complex behavior, we can mix ss and ll behavior in samples with odd numbers of columns, or can use vertical gradients in the amount of confinement to generate vertically moving domain walls. Finally, when many ss and ll rows (or all sl and ls rows) are confined, more complex discontinuous pattern transformations can take place in the bulk, which are sensitive to inhomogeneities and misalignments of the clamps.
We conclude that precise placement of the clamps, besides their degree of confinement, provide an additional, and easy to use, set of parameters to control the mechanical response of laterally constrained biholar metamaterials.